Aerosol radiative forcing and the accuracy of satellite aerosol optical depth retrieval

Petr Chylek[1] and Brad Henderson
Space and Remote Sensing Sciences, Los Alamos National Laboratory, Los Alamos, New Mexico, USA

Michael Mishchenko
Goddard Institute for Space Studies, NASA, New York, New York, USA

Received 4 August 2003; revised 8 September 2003; accepted 15 September 2003; published 18 December 2003.

[1] The minimum acceptable accuracy of the top of the atmosphere radiative flux of $\Delta F = 0.5$ W/m^2 leads to the required accuracy in satellite based aerosol optical depth (AOD) retrieval of about $\Delta\tau = 0.015$ over the land and $\Delta\tau = 0.010$ over the ocean. None of the current operational satellite based instruments for AOD retrieval has been able to achieve this accuracy. The RMSE (Root Mean Square Error) of the AVHRR (Advanced Very High Resolution Radiometer) is typically between 0.06 and 0.15, while the RMSE of the MODIS (Moderate resolution Imaging Spectroradiometer) over the land has been estimated to be $\Delta\tau = 0.05 + 0.2\tau$, which varies between $\Delta\tau = 0.07$ and $\Delta\tau = 0.21$ within the limit of usual aerosol optical depth between $\tau = 0.1$ and $\tau = 0.8$. The Department of Energy research satellite instrument, the Multispectral Thermal Imager (MTI), is capable of retrieving aerosol optical depth with an accuracy of $\Delta\tau = 0.03$ using an off nadir view at medium scattering angles. Theoretical analysis suggests that the uncertainties in aerosol phase function (due to uncertainties in aerosol shape, size distribution and optical properties) are the major obstacles for accurate aerosol optical depth retrieval. These uncertainties lead to a much larger error in aerosol optical depth retrieval at large scattering angles (usually at close to nadir view) than at off nadir views at medium scattering angles. On the basis of our theoretical analysis and on MTI experience, we suggest that in order to achieve the required accuracy in AOD retrieval, future satellite instruments using a single or dual-view AOD retrieval algorithm should use off-nadir views at medium scattering angles (between 50° and 100°). *INDEX TERMS:* 0305 Atmospheric Composition and Structure: Aerosols and particles (0345, 4801); 0360 Atmospheric Composition and Structure: Transmission and scattering of radiation; 1640 Global Change: Remote sensing; 1694 Global Change: Instruments and techniques; 3359 Meteorology and Atmospheric Dynamics: Radiative processes; *KEYWORDS:* aerosol optical depth, satellite retrieval, radiative forcing

Citation: Chylek, P., B. Henderson, and M. Mishchenko, Aerosol radiative forcing and the accuracy of satellite aerosol optical depth retrieval, *J. Geophys. Res.*, *108*(D24), 4764, doi:10.1029/2003JD004044, 2003.

1. Introduction

[2] The role of aerosols in climate and climate change is one of the largest uncertainties in our understanding of the present climate and in our abilities to predict future climate changes. Until the magnitude and the variability of anthropogenic aerosol radiative forcing are known, the predictions of future global warming may remain unacceptably high [*Hobbs et al.*, 1997]. The aerosols' direct effect involves their interaction with solar and terrestrial radiation [*Chylek and Coakley*, 1974; *Coakley and Cess*, 1985; *Charlson et al.*, 1992; *Kiehl and Briegleb*, 1993; *Chylek and Wong*, 1995; *Russell et al.*, 1999; *Sateesh and Ramanathan*, 2000]. The indirect effects include modification of the optical properties [*Twomey*, 1991; *Chylek et al.*, 1996] and life cycle of clouds [*Ramanathan et al.*, 2001; *Rotstayn and Lohmann*, 2002]. Though the mechanism of aerosol direct effect is theoretically well understood, an assessment of its magnitude is more difficult due to spatial and temporal aerosol variability.

[3] Remote sensing is the only means capable of providing global observational aerosol data that are needed for assessing aerosol induced radiative forcing at the top of the atmosphere (TOA). The aerosol optical depth (AOD) is the most important parameter needed for calculation of the aerosol TOA radiative forcing. The accuracy of the AOD retrieval using the Advanced Very High Resolution Radiometer (AVHRR) is between 0.05 and 0.15 in AOD [*Coakley et al.*, 2002]. The Moderate resolution Imaging Spectroradiometer (MODIS), provides the AOD (denoted by τ) with an estimated accuracy [*Remer et al.*, 2002; *Kaufman et al.*,

[1]Also at Department of Physics, New Mexico State University, Las Cruces, New Mexico, USA.

0148-0227/03/2003JD004044$09.00

1997] of $\pm(0.05 + 0.2\tau)$ over the land (the error varies between 0.07 and 0.21 with the AOD varying between 0.1 and 0.8), and $\pm(0.05 + 0.05\tau)$ over the ocean [*Remer et al.*, 2002].

[4] In this paper we present a theoretical study that suggests that uncertainty in aerosol optical properties, size distribution and particle shape leads to large errors when large scattering angles (usually near to a nadir view) are used for AOD retrieval. The errors are significantly smaller at medium scattering angles (usually at off nadir views). Comparison of the AOD retrieval using large and medium scattering angles with the Aerosol Robotic Network (AERONET) data suggests that the accuracy of the AOD retrieval is significantly improved by using medium scattering angles (off-nadir views). The accuracy of the AOD retrieval is expected to improve further by using satellite instruments capable of multiangle views of the target [*Flowerdew and Haigh*, 1996; *Veefkind et al.*, 1999; *North*, 2002; *Henderson and Chylek*, 2003].

2. What Accuracy of the AOD is Needed?

[5] To establish an appropriate standard of AOD accuracy for climate studies, we consider first the top of the atmosphere (TOA) radiative forcing due to carbon dioxide increase from preindustrial to the current level. According to the recent ICPP report [*World Meteorological Organization*, 2001] the carbon dioxide induced globally averaged TOA radiative forcing is estimated to be around 1.4 W/m^2. It seems reasonable that the accuracy of the aerosol TOA radiative forcing should be substantially lower than the forcing due to CO_2 increase between the preindustrial and the current concentration. We adopt the aerosol TOA radiative forcing uncertainty of $\Delta F = 0.5$ W/m^2 as a desirable limit on the forcing error.

[6] The radiative TOA forcing due to an optically thin aerosol layer can be derived for the case of a single scattering approximation [*Chylek and Wong*, 1995] in a simple analytical form:

$$F = -\frac{S_0}{4} T^+ T^- (1-N) 2\tau \Big[(1-a)^2 \beta\omega - 2a(1-\omega)\Big], \qquad (1)$$

where F is the TOA radiative forcing in W/m^2, S_0 is the incident solar flux at the top of the atmosphere, T^- and T^+ are the downward and upward atmospheric transmissions (from the TOA to the surface and back to the TOA), N is an average cloudiness, τ is an aerosol optical depth, a is the surface albedo, β is the fraction of the incident radiation scattered by an aerosol layer into the upward direction, and ω is the aerosol single scattering albedo.

[7] The uncertainty in aerosol TOA radiative forcing, ΔF, due to the uncertainty in AOD, $\Delta\tau$, is obtained as

$$\Delta F = \frac{\partial F}{\partial \tau}\Delta\tau = -2\frac{S_0}{4} T^+ T^- (1-N)\Big[(1-a)^2\beta\omega - 2a(1-\omega)\Big]\Delta\tau. \qquad (2)$$

To estimate the numerical value of the partial derivative of the radiative forcing F with respect to the aerosol optical depth, we use the nominal values of $S_0 = 1368$ W/m^2, $T^+T^- = 0.80$, $N = 0.5$, $a = 0.2$ for the land and $a = 0.05$ for the ocean, $\beta = 0.20$ and $\omega = 0.95$, from which we obtain $\partial F/\partial\tau = 29$ for the land and $\partial F/\partial\tau = 46$ over the ocean. These values compare reasonably well with 25 and 37 obtained by *Hobbs et al.* [1997] and 30 and 44 obtained by *Penner et al.* [1992] for the case of biomass burning aerosol.

[8] Adopting $\Delta F = 0.5$ W/m^2 as an acceptable accuracy of the TOA radiative forcing, from equation (2) we obtain the required accuracy of the AOD as

$$\Delta\tau = 0.016 \qquad (3a)$$

for an aerosol layer over the land, and

$$\Delta\tau = 0.011 \qquad (3b)$$

for an aerosol layer over the ocean. The desired AOD retrieval accuracy, given by equation (3), suggest that a considerable improvement in the satellite AOD retrieval is needed before any reliable conclusions concerning anthropogenic aerosol influence on the TOA radiative forcing and global climate can be established.

3. Major Sources of Error in the AOD Retrieval

[9] The fundamental equation connecting the satellite measured radiance, L, and the result of the radiative transfer model calculations can be written in the form

$$L = L_M + L_A + L_S, \qquad (4)$$

where L is the satellite measured radiance and L_M, L_A, and L_S stand for the radiance components produced by molecular, aerosol, and surface scattering, respectively. The sum $L_P = L_M + L_A$ is usually called the path radiance. All the radiances L, L_M, L_A, and L_S are explicit functions of the wavelength, λ, the solar zenith and azimuth angles, θ_0 and ϕ_0, the viewing zenith and azimuth angles, θ and ϕ; they are also implicit functions of all environmental variables (molecular atmosphere, aerosols, clouds and surface properties).

[10] The top of the atmosphere radiance component due to molecular scattering, L_M, can be calculated for a given geographical location from the surface pressure and temperature profile (measured or modeled) data.

[11] The TOA outgoing radiance due to aerosol scattering is generally obtained by solving the radiative transfer equation using an appropriate aerosol model. In the case of an optically thin aerosol layer ($\tau \ll 1$) the single scattering approximation can be used to obtain the aerosol path radiance, L_A, in an explicit form

$$L_A = \frac{F_0 \tau \omega p(\theta, \varphi, \theta_0, \varphi_0)}{4\pi \cos\theta}, \qquad (5)$$

where τ, ω, and p are the aerosol optical depth, single scattering albedo and the phase function, respectively.

[12] The TOA outgoing radiance due to surface reflection can be written in the form

$$L_S = \frac{F_0 \cos(\theta_0) T^-(\theta_0, \varphi_0) r_S T^+(\theta, \varphi)}{1 - r_S R_A}, \qquad (6a)$$

where F_0 is the incident solar flux at the top of the atmosphere, T^- is the transmission along the downward path toward the surface, T^+ is the transmission along the upward path from the surface to the satellite, r_S is the surface reflectance, and R_A is the atmosphere spherical albedo. For optically thin aerosol layers ($\tau \ll 1$), the multiple reflections between the surface and aerosol layer can be neglected and the surface reflected radiance can be written in a simplified form

$$L_S = F_0 \cos(\theta_0) T^-(\theta_0, \varphi_0) r_S T^+(\theta, \varphi), \tau \ll 1. \quad (6b)$$

The aerosol signal used for the AOD retrieval is in the L_A term. We rearrange the terms in equation (4) to obtain

$$L^* = L - L_M = \frac{F_0 \tau \omega p(\theta, \varphi, \theta_0, \varphi_0)}{4\pi \cos\theta} + F_0 \cos(\theta_0) T^-(\theta_0, \varphi_0) r_S T^+(\theta, \varphi). \quad (7)$$

The terms on the left-hand side of equation (7) are obtained from the satellite level measured radiances and from the molecular atmosphere model calculations. The right-hand side of equation (7) is a function of aerosol layer and surface properties. The first term on the right-hand side containing the aerosol optical depth carries aerosol signal from which the AOD is estimated. Therefore it is desirable to minimize the contribution of the second term (surface reflectance term) on the right-hand side of equation (7) by selecting pixels with low surface reflectance. In practice, pixels with dark vegetation, which means a high NDVI (normalized difference vegetation index) and low near infrared (2.2 μm) reflectivity are chosen. Although the surface reflectance term, L_S, is kept in our numerical calculation, for the purpose of our error analysis the L_S term will be neglected to facilitate simple analytical solution.

[13] From equation (7), the AOD can be written as

$$\tau = \frac{4\pi \cos(\theta) R^*}{\omega p(\theta, \varphi; \theta_0, \varphi_0)}, \quad (8)$$

where $R^* = (L - L_M)/F_0$ is the satellite observed reflectivity from which the reflectivity of purely molecular atmosphere has been subtracted. The largest uncertainty of the AOD retrieval arises from our lack of knowledge about the details of an aerosol layer. We do not know precisely the aerosol size distribution, particle shapes and orientation, and particle optical constants characterized by the real and imaginary parts of refractive index. All these environmental unknowns will affect the values of aerosol single scattering albedo and aerosol phase function. The error, $\Delta\tau$, introduced into the AOD due to the uncertainties $\Delta\omega$ and Δp is obtained from equation (8) in the form

$$\Delta\tau = -\tau\left(\frac{\Delta\omega}{\omega} + \frac{\Delta p}{p}\right). \quad (9)$$

The relative error in the single scattering albedo, $\Delta\omega/\omega$ is usually small ($\Delta\omega/\omega \ll 1$) and it does not depend on the sun and satellite viewing geometry. On the other hand, the relative error in the aerosol phase function, $\Delta p/p$, can be quite large. The magnitude of $\Delta p/p$ will also depend on the scattering angle corresponding to a particular sun and satellite position.

[14] In general, we can write

$$\frac{\Delta p}{p} = \frac{1}{p}\frac{\partial p}{\partial r_{\text{eff}}}\Delta r_{\text{eff}} + \frac{1}{p}\frac{\partial p}{\partial V_{\text{eff}}}\Delta V_{\text{eff}} + \frac{1}{p}\frac{\partial p}{\partial m_r}\Delta m_r + \frac{1}{p}\frac{\partial p}{\partial m_i}\Delta m_i + \frac{1}{p}\frac{\partial p}{\partial (sh)}\Delta(sh) + \ldots, \quad (10)$$

where the effective radius, r_{eff}, and effective variance, V_{eff}, specify the aerosol size distribution, m_r and m_i stand for the real and imaginary parts of the refractive index, and the shape factor, sh, designates the shape and the orientation of aerosol particles. The aerosol phase function, $p(\lambda, \theta_o, \phi_o; \theta, \phi)$, is of course also a function of the wavelength and solar and viewing zenith and azimuth angles.

[15] For a particular satellite-based AOD retrieval, the aerosol phase function cannot be calculated exactly, since the aerosol microphysical properties (size distribution, refractive indices, shape and orientation) are generally unknown. Although the use of suitable aerosol models aims at minimizing the error due to unknown aerosol properties, the aerosol phase function remains a major source of error in the AOD retrievals.

4. Aerosol Phase Function

[16] The aerosol phase function depends on the aerosol size distribution (effective radius and effective variance), the aerosol material (real and imaginary pars of refractive index) and the shape and orientation of the aerosol particles [*Mishchenko et al.*, 2002]. Figure 1 shows the aerosol phase function for spherical aerosol particles as a function of the scattering angle for various values of the imaginary part of refractive index (Figure 1a), real part of refractive index (Figure 1b), and for different size distributions characterized by varying effective radius (Figure 1c). The phase function is normalized as

$$\frac{1}{2}\int_0^\pi p(\Theta)\sin\Theta d\Theta = 1, \quad (11)$$

where Θ is the scattering angle [*Mishchenko et al.*, 2002].

[17] From Figure 1, it is apparent that the variations of the phase function (terms containing $\partial p/\partial r_{\text{eff}}$, $\partial p/\partial m_r$, $\partial p/\partial m_i$ in equation (10)) are larger at large scattering angles. Relative variations of the phase function (normalized to one at a scattering angle of 90°) with the change in the imaginary part of refractive index (Figure 2a), real part of refractive index (Figure 2b) and with respect to the effective radius of the size distribution (Figure 2c) are shown in Figure 2. It turns out that all aerosol uncertainty (size, real and imaginary part of refractive index) have a larger effect on the scattering phase function at large scattering angles between 100° and 180° than at moderate scattering angles between 50° and 100°. A similar dependence on the scattering angle has been found for the phase function as a function of the shape (Figure 3) of aerosol particles [*Mishchenko et al.*, 2002].

[18] The exact value of the ratio of the error in AOD of the close to nadir and off nadir view depends on a particular

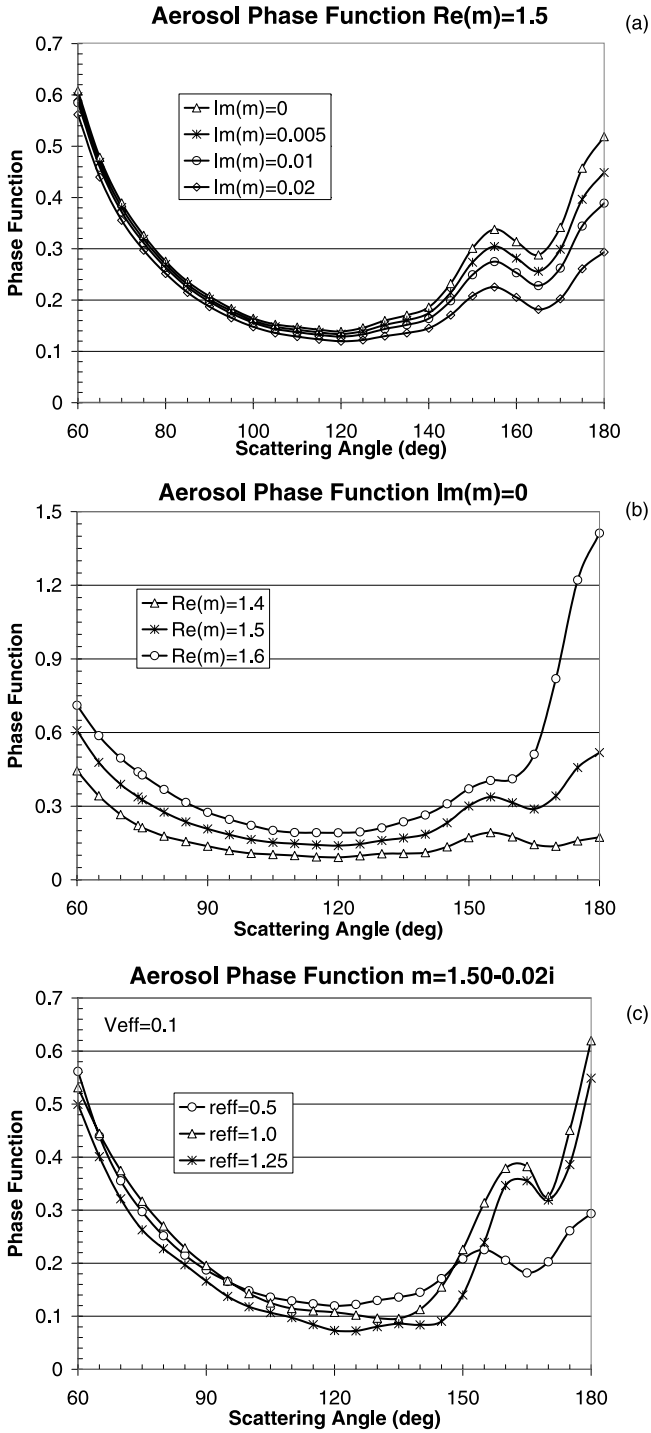

Figure 1. Aerosol phase function variations with the (a) imaginary and (b) real part of refractive index and (c) size distribution are larger at large scattering angles (100°–180°) than at medium (50°–100°) scattering angles. The phase function is calculated at the wavelength λ = 550 nm, for a power law aerosol size distribution with an effective radius r_{eff} = 0.5 μm and an effective variance v_{eff} = 0.1. The real part of the aerosol refractive index is m_r = 1.5. See color version of this figure in the HTML.

aerosol involved. However, in general the errors due to unknown aerosol parameters are smaller at medium scattering angles (50° < Θ < 100°) than at large scattering angles (100° < Θ < 180°). Consequently, the AOD retrieval at moderate scattering angles (off nadir look) will be more accurate than at large scattering angles (usually close to nadir look). Similarly, the two viewing angle algorithm that uses a close to nadir view will introduce a signal with a large noise that will partially negate the advantage of a double view

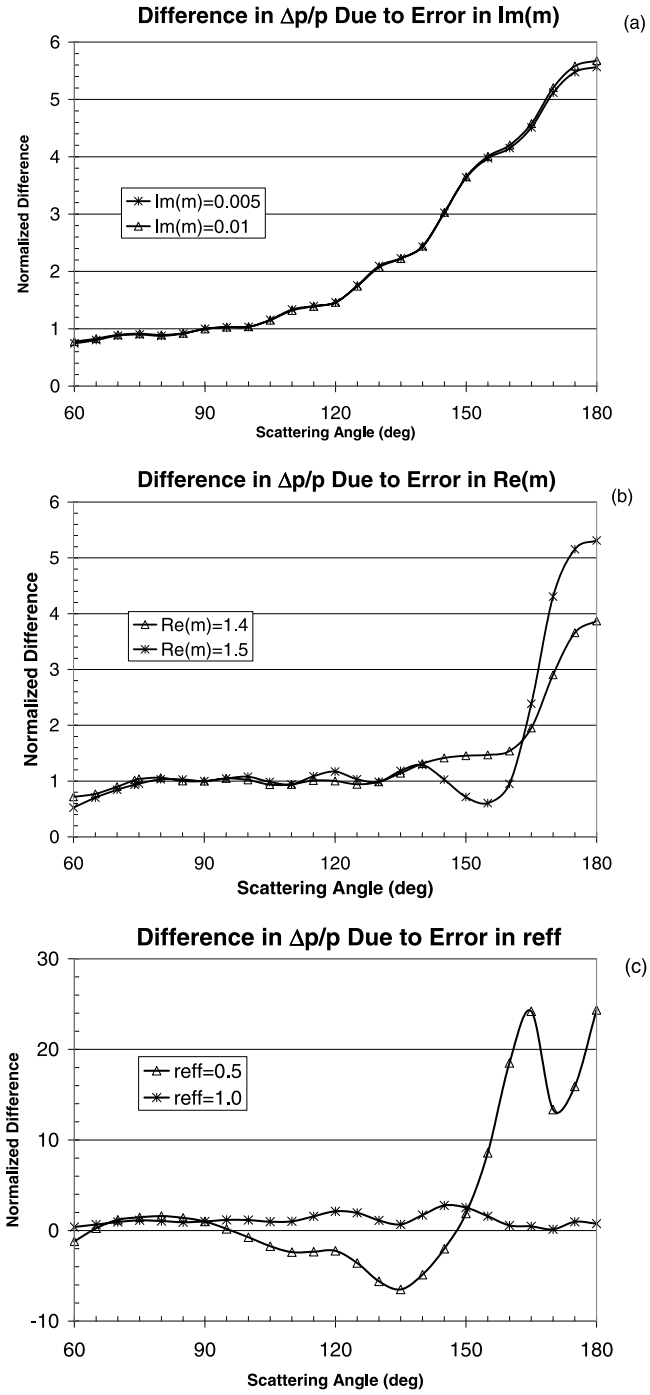

Figure 2. Differences in phase function (normalized to one at 90°) due to uncertainties in (a) imaginary and (b) real part of refractive index and (c) in the aerosol size distribution. See color version of this figure in the HTML.

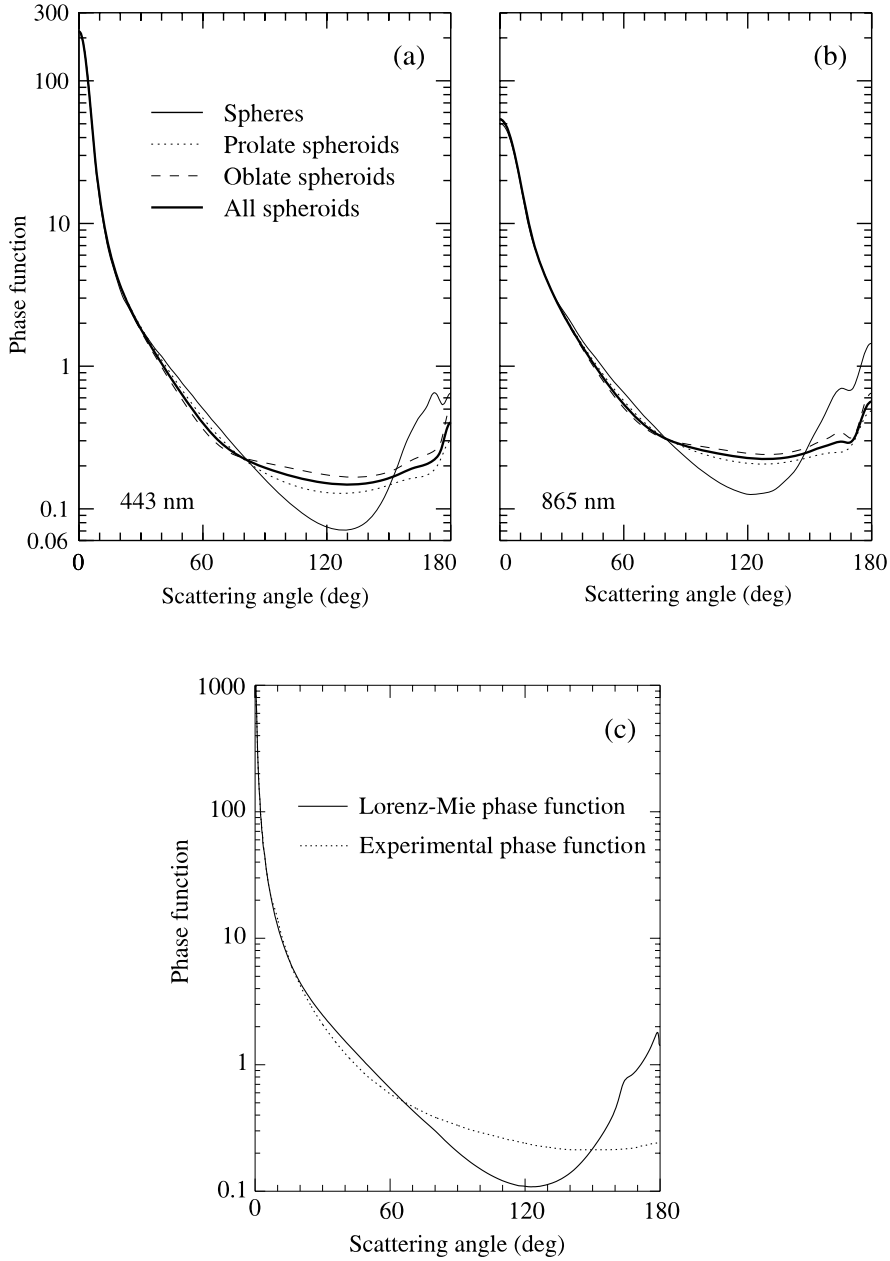

Figure 3. Aerosol phase function is affected by the shape of aerosol particles considerably more at large scattering angles than at medium angles. (a) and (b) Phase functions at 443 and 865 nm wavelengths for polydisperse spheres and shape mixtures of projected-area-equivalent randomly oriented prolate and oblate spheroids. The refractive indices are 1.53 + 0.0085i and 1.53 + 0.0012i, respectively. The size distribution is log normal with an effective radius of 1.163 μm [*Mishchenko and Travis*, 1997]. (c) Experimental phase function for randomly oriented quartz aerosols with an effective radius of 2.3 micrometers at a wavelength of 442 nm and the Lorenz-Mie phase function for projected-area-equivalent quartz spheres [*Mishchenko et al.*, 2003].

retrieval. On the other hand, a dual-angle view algorithm using two off nadir views, at scattering angles between 50° and 100°, should provide the most accurate AOD retrieval.

5. The MTI (Multispectral Thermal Imager) Data Set

[19] To provide experimental support for the above analysis, we analyze pairs of dual-view MTI images. The MTI is a DOE push broom multispectral satellite instrument [*Weber et al.*, 1999] with 15 spectral bands (Table 1) from visible to thermal infrared wavelengths. It was launched in March 2000 into a Sun-synchronous orbit at approximately 575 km altitude.

[20] The MTI pixel size is 5 m × 5 m in the visible and 20 m × 20 m in the infrared region; its swath width is around 12 km. The MTI has a dual view capability; the reflected solar radiances are measured close to nadir and

Table 1. List of Spectral Bands of the DOE Multispectral Thermal Imager

MTI Band	Central Wavelength, μm	Band Width, μm
A	0.484	0.057
B	0.558	0.066
C	0.650	0.050
D	0.810	0.086
E	0.874	0.025
F	0.940	0.056
G	1.015	0.048
H	1.376	0.027
I	1.646	0.193
O	2.224	0.271
J	3.787	0.565
K	4.957	0.174
L	8.225	0.334
M	8.656	0.379
N	10.471	0.456

then back along the track at a viewing angle around 60°. Two colocated images are generally taken within 2 min from each other. The change of the solar zenith angle is usually within 1 degree between the first and the second image.

[21] The MTI's small pixel size eliminates most errors in retrieval due to unresolved subpixel cloudiness. In addition to clear sky images, partially cloudy scenes can be used for retrieval as long as clouds or cloud shadows do not affect a considerable fraction of an image.

[22] The imagery used in our study was acquired over NASA Stennis Space Center (30°22′N, 89°37′W, about 20 m above mean sea level) between July 2000 and December 2001. The images were first screened for clouds to select clear and partially cloudy scenes suitable for analysis. We have used all available pairs of clear sky images and images with cloudiness lower than 15%. Altogether we have 28 images (14 pairs of near nadir and off nadir views) suitable for aerosol optical depth retrieval. The retrieved AOD is compared with AERONET AOD data acquired near the time of MTI overpass.

6. MTI Single-View and Double-View Retrieval

[23] Our single view retrieval is based on the algorithm of *Kaufman et al.* [1997] with appropriate modification for use with the MTI available bands. The first step of the retrieval is to find dark pixels. Within the given image the algorithm selects pixels with high values of the normalized vegetation index and with low reflectivity in the 2.2 μm (MTI "O" band) channel. Next, using the satellite level observed radiances, we estimate the surface reflectance in the MTI O band, where the aerosol effect is considerably smaller than at visible wavelength (due to an approximate inverse wavelength dependence of the aerosol scattering cross sections). Then, using the correlation between the vegetation ground reflectance [*Kaufman et al.*, 1997] at infrared (2.2 μm) and visible wavelengths, the ground reflectance at visible wavelengths is estimated. Finally from the measured radiances and the estimated ground reflectance at visible wavelengths, the aerosol optical thickness at 550 nm is deduced using the 6s radiative transfer code [*Vermote et al.*, 1997] for a given set of environmental variables and sun/satellite geometry.

[24] Our double-view AOD retrieval algorithm is based on equation (4) with a simplified surface reflection term given by equation (6b) in which the multiple reflections between the aerosol layer and the surface are neglected. Dividing equation (4) by incoming solar flux, we can write

$$R_1 = R_{1M} + R_{1A} + r_{1S} T_1^- T_1^+ \tag{12a}$$

$$R_2 = R_{2M} + R_{2A} + r_{2S} T_2^- T_2^+, \tag{12b}$$

where the subscripts 1 and 2 refer to the two viewing angles, R is an apparent reflectivity as observed by the satellite, R_M and R_A are reflectivity due to the molecular atmosphere and aerosol layer, and r_S is the surface reflectivity.

[25] Making an additional assumption that the ratio, k, of the surface reflectivities at the considered two viewing angles is a constant for a given Sun and viewing geometry and for the used wavelengths in the visible and near IR (2.2 μm)

$$k = \frac{r_{2S}}{r_{1S}}, \tag{13}$$

we can eliminate the unknown reflectivities r_{1S} and r_{2S} from equation (12) to obtain

$$\frac{R_1 - R_{1M} - R_{1A}}{T_1^- T_1^+} = \frac{R_2 - R_{2M} - R_{2A}}{k T_2^- T_2^+}. \tag{14}$$

The same final equation was derived from a slightly different set of assumptions by *Veefkind et al.* [1998].

[26] The molecular and aerosol scattering cross sections decrease with the wavelength approximately as λ^{-4} and λ^{-1}, respectively. Consequently, the molecular and aerosol scattering terms, R_M and R_A, can be neglected for MTI's O band, centered at 2.2 μm, and the constant k can be obtained as the ratio of band O reflectances at the two viewing angles. Since the ratio k depends on the sun and viewing geometry, the determination of k has to be done separately for each considered image. In our set of images, k varied between 0.8 and 1.2.

[27] Next, equation (14) was solved numerically (for a short wavelength red band), by calculating each side for a set of AODs until the agreement between the left-hand side and right-hand side was achieved. We have selected 50 dark vegetation pixels in each image for which we have retrieved the AOD. The results were averaged to determine the AOD for a particular image pair.

7. Results

[28] To evaluate the accuracy of the single-view and double-view aerosol optical depth retrievals, we need to compare the satellite derived optical thickness with other AOD measurements of known quality that are taken at the same location within a short time of the satellite image. For that reason we have chosen the NASA Stennis Space Center site where the AERONET (Aerosol Robotic Network) Sun photometer [*Holben et al.*, 1998] provides almost simultaneous high accuracy measurements of AOD. The AERONET level 2 and 1.5 data are expected to have an accuracy of about 10%. Images with time differences of more than

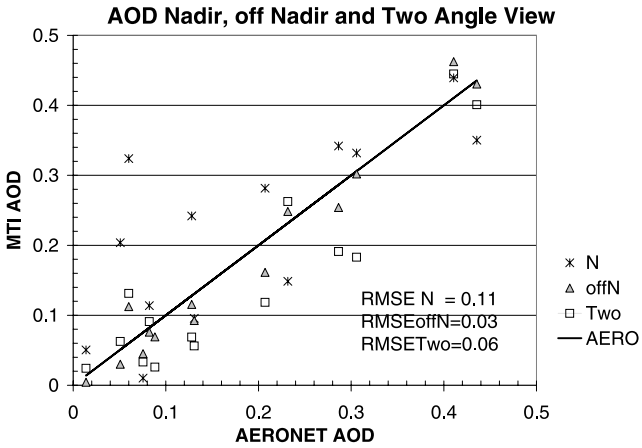

Figure 4. Comparison of the MTI aerosol optical depth retrieval using a single-view both nadir and off-nadir and a dual-view algorithm. See color version of this figure in the HTML.

two hours were not considered suitable for the validation (most of the images are taken within 20 min from the available AERONET AOD measurements).

[29] The results of our AOD retrieval are shown in Figure 4. The single view close to nadir algorithm leads to a considerable error of the AOD retrieval. The RMSE (root mean square error) defined as

$$\mathrm{RMSE} = \sqrt{b^2 + \sigma^2} \tag{15}$$

(where b and σ stand for the mean and the standard deviation of the difference between the retrieved and AERONET AOD) is 0.11 in units of AOD. The dual-view algorithm improves the accuracy of the AOD retrieval by about a factor of two; the RMSE of the dual-view algorithm is 0.06 in AOD units. However, the best accuracy is achieved by using the single-view algorithm at off nadir view [*Chylek et al.*, 2003] at moderate scattering angles. The RMSE error of the single off nadir view is 0.03 in aerosol optical depth (Figure 4).

8. Conclusion and Discussion

[30] We suggest that the maximum error in aerosol optical depth that will still let us make a meaningful statement concerning the aerosol climate effect is around $\Delta\tau = 0.015$ over the land and $\Delta\tau = 0.010$ over the ocean. This error in AOD produces a top of the atmosphere radiative forcing error of about 0.5 W/m^2 (for comparison the increase of carbon dioxide from the preindustrial to the current level produces a TOA radiative forcing of around 1.4 W/m^2).

[31] It seems that neither the AVHRR nor the MODIS instrument is able to achieve this accuracy (an improvement of accuracy by a factor of four to six would be needed). Our analytical treatment suggests that the major disadvantage of the current instruments is that they use a close to nadir view for AOD retrieval. A considerable improvement of the AOD retrieval (by about a factor of two to three) should be possible using a single off nadir view (scattering at moderate scattering angles, preferably in the range of 50° to 100°). An additional improvement can be expected using a double-view retrieval algorithm that utilizes two off nadir (medium scattering angles) views and incorporating polarization measurements [*Mishchenko and Travis*, 1997; *Chowdhary et al.*, 2001].

[32] Our analysis of the DOE MTI pairs of double-view images suggests that the use of the off nadir view can significantly improve the accuracy of the AOD retrieval (from 0.11 to 0.03 in AOD for a set of analyzed images). The current MISR (Multiangle Imaging Spectroradiometer) instrument [*Diner et al.*, 2001; *Martonchik et al.*, 2002] might be able to approach the proposed accuracy (equations (3) with a dual-view algorithm using two off nadir views with scattering angles between 50° and 100° (since the MISR does not have an appropriate near infrared band corresponding to the MTI O band, a different dual-view algorithm has to be developed). To improve the accuracy of future AOD retrievals, the next generation of operational satellite instruments should utilize the off nadir viewing geometry (at medium scattering angles) for AOD retrieval.

[33] **Acknowledgments.** We thank C. Borel and A. Davis for helpful discussions. The reported research was partially supported by the U.S. DOE as a part of the Atmospheric Radiation Measurement Program.

References

Charlson, R. J., S. E. Schwartz, J. M. Hales, R. D. Cess, J. A. Coakley, J. E. Hansen, and D. J. Hofman, Climate forcing by anthropogenic aerosols, *Science*, *255*, 423–430, 1992.

Chowdhary, J., B. Cairns, M. Mishchenko, and L. Travis, Retrieval of aerosol properties over the ocean using multispectral and multiangle photopolarimetric measurements from the research scanning polarimeter, *Geophys. Res. Lett.*, *28*, 243–246, 2001.

Chylek, P., and J. A. Coakley, Aerosol and climate, *Science*, *183*, 75–77, 1974.

Chylek, P., and J. Wong, Effect of absorbing aerosol on global radiation budget, *Geophys. Res. Lett.*, *22*, 929–931, 1995.

Chylek, P., G. Lesins, G. Videen, J. Wong, R. Pinnick, D. Ngo, and J. Klett, Black carbon and absorption of solar radiation by clouds, *J. Geophys. Res.*, *101*, 23,365–23,371, 1996.

Chylek, P., B. Henderson, and M. Mishchenko, Satellite based retrieval of aerosol optical thickness: The effect of sun and satellite geometry, *Geophys. Res. Lett.*, *30*(11), 1553, doi:10.1029/2003GL016917, 2003.

Coakley, J. A., and R. D. Cess, Response of the NCAR community climate model to the radiative forcing of the naturally occurring tropospheric aerosols, *J. Atmos. Sci.*, *42*, 1677–1692, 1985.

Coakley, J. A., Jr., W. R. Tahnk, A. Jayaraman, P. K. Quinn, C. Devaux, and D. Tanré, Aerosol optical depths and direct radiative forcing for INDOEX derived from AVHRR: Theory, *J. Geophys. Res.*, *107*(D19), 8009, doi:10.1029/2000JD000182, 2002.

Diner, D. J., et al., MISR aerosol optical depth retrievals over southern Africa during the SAFARI-2000 dry season campaign, *Geophys. Res. Lett.*, *28*, 3127–3130, 2001.

Flowerdew, R. J., and J. D. Haigh, Retrieval of aerosol optical thickness over land using the ATSR-2 dual look radiometer, *Geophys. Res. Lett.*, *23*, 351–354, 1996.

Henderson, B., and P. Chylek, Comparison of a single-view and a double-view aerosol optical depth retrieval algorithm, *Proc. SPIE*, *5157*, in press, 2003.

Hobbs, P. V., J. S. Reid, R. A. Kotchenruther, R. J. Ferek, and R. Weiss, Direct Radiative Forcing by Smoke from Biomass Burning, *Science*, *275*, 1776–1778, 1997.

Holben, B. N., et al., AERONET—A federated instrument network and data archive for aerosol characterization, *Remote Sens. Environ.*, *66*, 1–16, 1998.

Kaufman, Y. J., D. Tanre, L. A. Remer, E. F. Vermote, and A. Chu, Operational remote sensing of tropospheric aerosol over land from EOS moderate resolution imaging spectroradiometer, *J. Geophys. Res.*, *102*, 17,051–17,067, 1997.

Kiehl, J. T., and B. P. Briegleb, The relative roles of sulfate aerosols and greenhouse gases in climate forcing, *Science*, *260*, 311–314, 1993.

Martonchik, J. V., D. J. Diner, K. A. Crean, and M. A. Bull, Regional aerosol retrieval results from MISR, *IEEE Trans. Geosci. Remote Sens.*, *40*, 1520–1531, 2002.

Mishchenko, M. I., and L. D. Travis, Satellite retrieval of aerosol properties over the ocean using polarization as well as intensity of reflected sunlight, *J. Geophys. Res.*, *102*, 16,989–17,013, 1997.

Mishchenko, M. I., L. D. Travis, and A. A. Lacis, *Scattering, Absorption, and Emission of Light by Small Particles*, Cambridge Univ. Press, New York, 2002.

Mishchenko, M. I., I. V. Geogdzhayev, L. Liu, J. A. Ogren, A. A. Lacis, W. B. Rossow, J. W. Hovenier, H. Volten, and O. Muñoz, Aerosol retrievals from AVHRR radiances: Effects of particle nonsphericity and absorption and an updated long-term global climatology of aerosol properties, *J. Quant. Spectrosc. Radiat. Transfer*, *79/80*, 953–972, 2003.

North, P. R. J., Estimation of aerosol opacity and land surface bidirectional reflectance from ATSR-2 dual-angle imagery: Operational method and validation, *J. Geophys. Res.*, *107*(D12), 4149, doi:10.1029/2000JD000207, 2002.

Penner, J. E., R. E. Dickinson, and C. A. O'Neil, Effects of aerosol from biomass burning on the global radiation budget, *Science*, *256*, 1432–1434, 1992.

Ramanathan, V., P. J. Crutzen, J. T. Kiehl, and D. Rosenfeld, Aerosols, climate and the hydrological cycle, *Science*, *294*, 2119–2124, 2001.

Remer, L., Y. J. Kaufman, Z. Levin, and S. Ghan, Model assessment of the ability of MODIS to measure top-of-atmosphere direct radiative forcing from smoke aerosol, *J. Atmos. Sci.*, *59*, 657–667, 2002.

Rotstayn, L. D., and U. Lohmann, Tropical rainfall trends and the indirect aerosol effect, *J. Clim.*, *15*, 2103–2116, 2002.

Russell, P. B., P. V. Hobbs, and L. L. Stowe, Aerosol properties and radiative effects in the U. S. east coast haze plume: An overview of the tropospheric aerosol radiative forcing observational experiment (TARFOX), *J. Geophys. Res.*, *104*, 2213–2222, 1999.

Sateesh, S. K., and V. Ramanathan, Large differences in tropical aerosol forcing at the top of the atmosphere and Earth's surface, *Nature*, *405*, 60–63, 2000.

Twomey, S., Aerosols, clouds and radiation, *Atmos. Environ., Part A*, *25*, 2435–2442, 1991.

Veefkind, J. P., G. de Leeuw, P. A. Durkee, P. B. Russell, P. V. Hobbs, and J. M. Livingston, Aerosol optical depth retrieval using the ATSR-2 and AVHRR data during TARFOX, *J. Geophys. Res.*, *104*, 2253–2260, 1999.

Vermote, E. F., D. Tanré, J. L. Deuzé, M. Herman, and J. J. Morcrette, Second simulation of the satellite signal in the solar spectrum: An overview, *IEEE Trans. Geosci. Remote Sens.*, *35*, 675–686, 1997.

Weber, P. G., C. C. Borel, W. B. Clodius, B. J. Cooke, and B. W. Smith, Design considerations, modeling and analysis for the Multispectral Thermal Imager, in *Proc. SPIE*, *3701*, paper, 3701–3713, 1999.

World Meteorological Organization, IPCC report, third assessment, Geneva, 2001.

P. Chylek and B. Henderson, Space and Remote Sensing Sciences, Los Alamos National Laboratory, Mail Stop B244, Los Alamos, NM 87545, USA. (chylek@lanl.gov)

M. Mishchenko, Goddard Institute for Space Studies, 2880 Broadway, New York, NY 10025, USA. (crmim@giss.nasa.gov)